HOKKAIDO UNIVERSITY

Title	Risk assessment of forest disturbance by typhoons with heavy precipitation in northern Japan
Author(s)	Morimoto, Junko; Aiba, Masahiro; Furukawa, Flavio et al.
Citation	Forest ecology and management, 479, 118521 https://doi.org/10.1016/j.foreco.2020.118521
Issue Date	2021-01-01
Doc URL	https://hdl.handle.net/2115/87596
Rights	© 〈2021〉. This manuscript version is made available under the CC-BY-NC-ND 4.0 license http://creativecommons.org/licenses/by-nc-nd/4.0/
Rights(URL)	https://creativecommons.org/licenses/by-nc-nd/4.0/
Type	journal article
File Information	2016WT_ms.pdf, 本文

Risk assessment of forest disturbance by typhoons with heavy precipitation in northern

Japan

Junko Morimoto[*,a], Masahiro Aiba[b], Flavio Furukawa[a, d], Yoshio Mishima[c], Nobuhiko

Yoshimura[a, d], Sridhara Nayak[e], Tetsuya Takemi[e], Haga Chihiro[f], Takanori Matsui[f], Futoshi

Nakamura[a]

[a]Graduate School of Agriculture, Hokkaido University, Sapporo, Hokkaido, 060-8587, Japan

[b]Research Institute for Humanity and Nature, Kyoto, 603-8047, Japan

[c]Faculty of Geo-Environmental Science, Rissho University, Kumagaya, Saitama, Japan

[d]Department of Environmental and Symbiotic Science, Rakuno Gakuen University, Ebetsu 069-

8501, Japan

[e]Disaster Prevention Research Institute, Kyoto University, Gokasho, Uji, Kyoto, 611-0011,

Japan

[f]Division of Sustainable Energy & Environmental Engineering, Graduate School of Engineering,

Osaka University, Suita, Osaka, 565-0871, Japan

*Corresponding author

Junko MORIMOTO

Graduate School of Agriculture, Hokkaido University, Kita 9, Nishi 9, Kita ku, Sapporo,

21   Hokkaido, 060-8587, Japan

22   E-mail: jmo1219@for.agr.hokudai.ac.jp

23   Tel.: +81-11-736-7735

24

25   Author contributions

29

30 **Abstract**

31 Under future climate regimes, the risk of typhoons accompanied by heavy rains is expected to

32 increase. Although the risk of disturbance in forest stands by strong winds has long been of

33 interest, we have little knowledge of how the process is mediated by storms and precipitation.

34 Using machine learning, we assess in cool- temperate forests the disturbance risk by typhoons

35 that landed in northern Japan in late August 2016 to determine the features of damage due to

36 typhoons accompanied by heavy precipitation, discuss how the process is mediated by

37 precipitation as inferred from the modelling results, and delineate the effective solutions for

38 forest management to decrease the future risk in silviculture. In the results, we confirmed two

39 types of behaviours in the model: one represents the same process as that of forest disturbance by

40 the strong wind, which has been widely studied, and another represents a unique process

41 mediated by storms and precipitation, which has not been investigated. Specifically, the ridges

42 that received strong wind from the front side had the highest risk of disturbance. Precipitation

43 increased the probability of disturbance in forest stands, and its effect depended on the dominant

44 species composition. Our hypothesis regarding treefall mediated by storms and precipitation is

45 that rainwater flows into the gaps around the tree root systems during sway, and the introduction

46 of rainwater below the root-soil plate decreases the root anchorage. The species-specific

47 vulnerability to rainfall may depend on the volume of lateral roots. Modelling the disturbance

48 risk helped us to examine the kinds of factors that were related to exposure and vulnerability that

49 should be managed to effectively decrease the risk of disturbance by typhoons during future

50 uncontrollable hazards. It is recommended to avoid silviculture on the ridges of plateaus

51 considering the high risk estimated in this area. In addition, species with dense lateral roots

52 would be suitable for planting because they may have high resistance to typhoons with heavy

2

53   precipitation.

54

55

57

58

1 Introduction

Extremely intense tropical cyclones (categories 4 and 5; maximum wind speed ≥ 69 m·s^{-1}) are expected to increase in frequency at the end of the twenty-first century (2075–99) under the Intergovernmental Panel on Climate Change (IPCC) A1B scenario (Murakami et al., 2012). This timescale corresponds to the time when the planted seedlings reach old age and become vulnerable to strong winds in the temperate zone. Tropical cyclones (typhoons) in Eastern Asia sometimes bring heavy rain; Typhoon Morakot in 2009 (over 3000 mm) and Typhoon Talas in 2011 (over 2000 mm) in the western North Pacific region are recent examples that induced extreme rainfall. Several case studies have indicated that precipitation accompanied by a typhoon is expected to be intensified in future climates (for example, Nayak and Takemi, 2019a, 2019b; Takemi, 2019). We should be aware of the increased disaster risk in forest landscapes caused by both strong winds and extreme precipitation in the regions where typhoons are a major natural hazard to forest ecosystems (Nakashizuka, 1989; Yamamoto, 1989).

Risks from climate change impacts result from the interaction of vulnerability, exposure, and hazards (Oppenheimer et al., 2014). In the case of forest damage caused by typhoons, hazards correspond to strong winds and heavy rain, exposure implies the presence of forest ecosystems in places and settings that could be damaged, and vulnerability is the susceptibility of the forest structure to strong winds and heavy rain. All factors related to risk must be considered when analysing the process of emergent risks. Forest disturbance risk models consisting of factors representing hazard, exposure, and vulnerability will also be useful for finding an effective adaptation measure because these models will help us to examine the factors of exposure and vulnerability that will be effective in decreasing the risk under uncontrollable hazards.

4

82   Many previous studies have empirically examined windthrow in forest stands and

83   revealed the effects of various factors related to hazards, exposure, and vulnerability. High ridges

84   that run perpendicular to prevailing storm directions protect leeward slopes and valley positions

85   (Kramer et al., 2001). However, when the valley line and wind direction are parallel, the wind

86   will converge along the terrain, and damage will occur along the valley floor (Ruel et al., 1998).

87   The probability of disturbance is also highly dependent on the forest structure. Homogeneous

88   forest stands with trees of the same age, species, and height and with the same arrays have a

89   higher probability of damage than heterogeneous forest stands (Jalkanen and Mattila, 2000;

90   Mitchell et al., 2001; Morimoto et al., 2019), probably because these stands allow strong winds

91   to pass through forest stands while maintaining their high speed.

92   However, we have little knowledge of how the process of forest disturbance is mediated

93   by storms and heavy rain, which will be a challenge to address under the changing climate. Some

94   studies on forest disturbance in relation to the constant wet condition of soil suggest that shallow

95   rooting depths due to high water tables contribute to the constant high risk of windthrow

96   (Stathers et al., 1994; Mitchell et al., 2001). However, few studies have succeeded in

97   incorporating the ephemeral effect of precipitation into forest disturbance models (Mitchell and

98   Ruel, 2015).

99   During 14 days in late August 2016, four typhoons crossed Hokkaido, the northern part of

100   Japan, and a total of 9,000 ha of forest was damaged by windthrow and landslides (Bureau of

101   Forestry, Department of Fisheries and Forestry, Hokkaido Government, 2018). The maximum

102   wind speed of over 35 m·s^{-1} was recorded mainly in the southern part of Hokkaido, and the

103   maximum monthly precipitation was updated at 89 points of the 225 meteorological observation

104   points in Hokkaido (Japan Meteorological Agency). These successive typhoons were

105   accompanied by heavy rainfall and are recognized as a typical example that might frequently

106   occur in the future (Takemi, T., 2019). Then, we built a prediction model to estimate the forest

107   disturbance probability due to typhoons accompanied by heavy rain with hazard, exposure, and

108   vulnerability parameters to (1) identify the features of forest disturbance caused by typhoons

109   accompanied by heavy precipitation, (2) discuss how the disturbance process is mediated by

110   precipitation as inferred from the models and (3) delineate effective solutions in forest

111   management to decrease the risk in silviculture in the future. We used gradient boosted decision

112   trees (GBDTs), a machine learning method, to model the forest disturbance risk.

113

114   **2 Material and methods**

115

116   *2.1 Study area*

117   Our study focused on 325 km^2 of cool temperate forests in Setana, Hokkaido, Japan (Fig. 1;

118   41°22.6'N, 139°58'E). This region includes a variety of terrain from flat plains to steep

119   mountains, with altitudes from 0 m to 1300 m. The mean annual temperature in the study area is

120   8.8 °C, and the mean annual precipitation is 1,055.9 mm (Japan Meteorological Agency;

121   averages for the period 1981–2010). Andosols and brown forest soils were found within the

122   study region, which was dominated by natural forests of *Fagus crenata* Blume, *Betula ermanii*

123   Cham., and *Acer pictum* Thunb. and plantation forests of *Abies sachalinensis* (F. Schmidt) Mast.

124   and *Larix kaempferi* (Lamb.) Carrière.

125
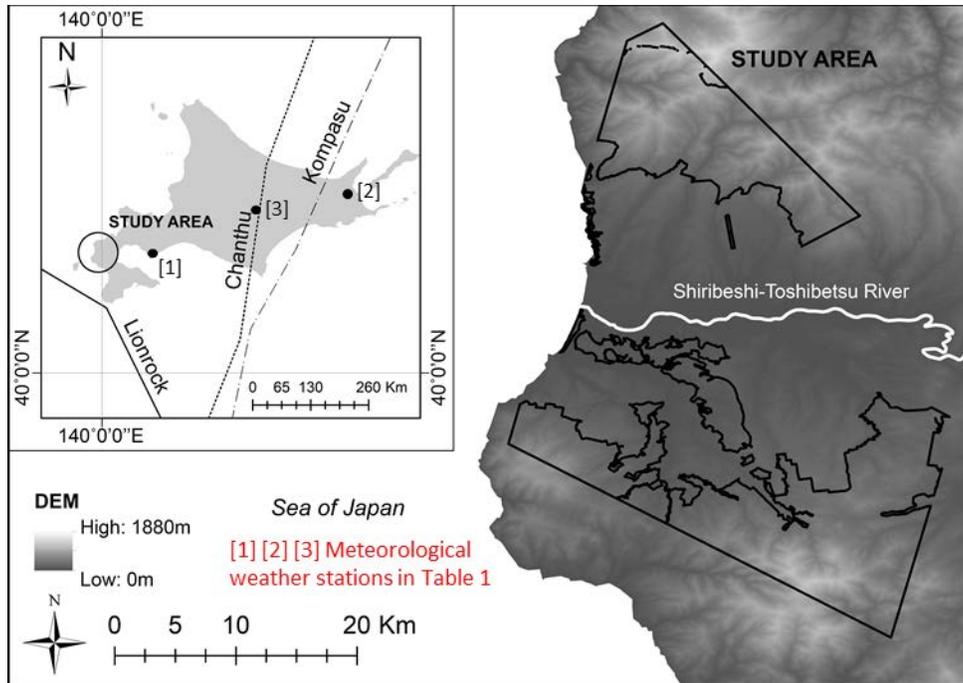
Fig. 1. Study area and tracks of typhoons.

127

2.2 Typhoons landed in the study area in August 2016

Four typhoons accompanied by heavy precipitation landed on or came close to Hokkaido over

the 14 days from August 17th to August 30th (Table 1) and caused significant damage to

transportation infrastructure, aquaculture, agriculture, and forestry. Among these typhoons,

Chanthu (No. 7, landing on August 17th), Kompasu (No. 11, landing on August 21st), and

Lionrock (No. 10, landing on August 30th) affected the study area and caused extensive

windthrow and landslides. We focused on the windthrow, especially for the forest collapse which

consisted of many fallen trees uprooted and broken trunks without crowns and a few surviving

trees. The damage to trees was mostly uprooting, and broken trunks sustained minor damage

(uprooted: broken trunks = 7: 3, Supplemental Material S2). The total amount of precipitation

over 500 mm was recorded during this period at many meteorological observatories, which is

7

139   two to four times greater than the amount of precipitation received in an average year (Japan

140   Meteorological Agency, 2017).

141   **Table 1.** General weather conditions during the period of typhoon landing.

	Typhoon features during landfall			Precipitation accompanied by typhoon			
			Max wind speed			Max total precipitation in Hokkaido	
Name of typhoon	Landing period in Hokkaido	Min central pressure (hPa)	(mrs-1)	Precipitation period	(mm)	Meteorological weather station recorded [sign on Figure 1]	Location and altitude of the station
Chanthu	Aug. 17th	980	30	Aug. 16-18th	242.5	Nakakineusu [1]	42°13.4'N, 142°56.9'E, 80m
Kompasu	Aug. 21st	994	18	Aug. 20-23rd	296	Itokushibetsu [2]	43°43.3'N, 144°59.3'E, 115m
Linrock	Aug. 30th	940	45	Aug. 26-31st	373	Nukabira [3]	43°22.0'N, 143°11.5'E, 540m

142   The record is cited from the report by the Japan Meteorological Agency (2016).

143   *2.3 Windthrow mapping*

144   PlanetScope satellite imagery (Planet Lab Inc., 2020) was used for windthrown mapping. The

145   satellites deliver images with a spatial resolution of 3 m per pixel in four different spectral bands:

146   blue (455 – 515 nm), green (500 – 590 nm), Red (590 – 670 nm), and near infrared (780 – 860

147   nm). The temporal resolution was approximately daily with a constellation operation of more

148   than 130 satellites, which was crucial for vegetation change detection analysis (Guangxing

149   Wang, 2013). We used the Level3B product, which was already orthorectified and

150   radiometrically calibrated to surface reflectance. Before the study, we ensured that windthrown

151   areas could be identified in the PlanetScope satellite imagery (Supplementary material S1). We

152   used pre-typhoon images collected on June 28th and July 1st, 2016, depending on the region, and

153   post-typhoon images collected on September 21, 2016, through the PlanetScope platform. The

154   images pre- and post-typhoons were individually combined to cover the study area.

155   The spectral angle mapper (SAM) algorithm was used to detect windthrow areas. The

156   SAM is a spectral classification algorithm that calculates the spectral similarity based on the

8

157   spectral angle between pixels of an input image and training samples (Kruse et al., 1993). First,

158   we created an input image that has ten spectral bands by layer stacking the spectral bands from

159   the pre-typhoon (4 bands) and post-typhoon (4 bands) images plus normalized difference

160   vegetation index (NDVI) bands calculated from each image (2 bands). Windthrown areas should

161   have their specific spectral characteristics in the input image (Coppin and Bauer, 1996). Next, we

162   created training samples of windthrown areas through visual interpretation comparing the post-

163   typhoon image with the pre-typhoon image. These images were created in obvious windthrown

164   areas. Finally, we detected windthrown areas using the input image and training samples through

165   the SAM algorithm on the Semi-Automatic Classification Plugin (Congedo, 2016) within QGIS

166   3.02 (QGIS.org, 2020) (Supplementary material S1). With the SAM method, there is a possibility

167   that land use with spectral characteristics remarkably similar to a windthrow, such as grassland,

168   will be erroneously classified to be windthrow. However, since our methods use the spectral

169   features before and after the typhoons for the classification, such a probability is rare.

170   The test data for accuracy assessment of the windthrow mapping were created using 100

171   random samplings, which were visually interpreted in the same way as the training sample. In

172   addition, the post-typhoon WorldView2 imagery (August 20th, 2017), which provides a higher

173   spatial resolution of 0.37 cm/px, was used as a reference image. The assessment results of the

174   accuracy of the windthrow mapping revealed a substantial level of agreement (kappa = 0.8,

175   overall accuracy in the confusion matrix = 90 %). The total windthrow area within the study

176   region was approximately 240 ha, with a mean patch size of 0.038 ha (maximum = 7.16 ha,

177   minimum = 0.01 ha).

178

179   *2.4 Preparing the dataset for modelling*

9

180   The study area of 325 km^2 was divided into 10 m × 10 m grid cells using geographic information

181   systems. For modelling, all 16,472 positive (forest disturbance) cases and 49,416 randomly

182   sampled (three-fold of the positive cases) negative cases were used. The estimated value of the

183   probability by modelling did not indicate the actual probability of forest disturbance at this event

184   but rather its relative probability. As for explanatory variables, we firstly selected the crucial

185   factors identified by previous studies focused on windthrow risk assessments in mountainous

186   region dominated by cool-temperate and boreal forests (Kramer et al., 2001; Mitchell et al.,

187   2001; Nakajima et al., 2009). In addition to it, we selected series of precipitation indicators

188   identified by previous study focusing on shallow landslide in forests by heavy rainfall (Dou et

189   al., 2019). After the preliminary analyses, variables whose contributions were limited were

190   omitted from the final model for ease of interpretation. Then seventeen explanatory variables

191   were considered in this study as follows: meteorological hazard factors (n = 6): maximum wind

192   speed of typhoon Mindulle (m·s^{-1}), maximum wind speed of typhoon Linrock (m·s^{-1}), duration of

193   wind speed ≥ 15 m·s^{-1} during typhoon Linrock (m·s^{-1}), maximum wind speed of typhoon

194   Chanthu (m·s^{-1}), duration of wind speed ≥ 15 m·s^{-1} during typhoon Chanthu (m·s^{-1}), and total

195   rainfall during the typhoon period (mm); topographical exposure factors (n = 6): surface geology

196   type, slope angle (°), topex (topographic exposure index, Miller et al., 1987; explained later) with

197   a 1 km line length, topex with a 2 km line length, topex with a 3 km line length, and the slope

198   direction relative to the wind of the highest speed (°, 0=head on, 180=opposite); and forest

199   vulnerability factors (n = 5): forest type (planted or natural), stand age (years), mean diameter at

200   breast height (DBH) of the dominant species (cm), dominant forest species of the forest stand)

201   and stand volume per 100 m^2 (m^3).

202

203   For the calculation of the maximum wind speed and the duration of wind speed ≥ 15 m·s$^-$

204   ^{1} of typhoons Chanthu, Kompasu, and Linrock, the Advanced Research Weather Research and

205   Forecasting (WRF) model (Skamarock et al., 2008) with two-way configuration and four nested

206   domains with 9 km, 3 km, 1 km and 200 m resolutions was used to numerically simulate the

207   three typhoons and the surrounding meteorological fields. The criterion of wind speed ≥ 15 m·s^{-1}

208   is the threshold of strong winds due to typhoons by the Japan Meteorological Agency (JMA)

209   definition, which is slightly lower than the threshold 17.2 m·s^{-1} of tropical storms by World

210   Meteorological Agency (WMA) definition. The meteorological simulations for typhoon Chanthu

211   and typhoon Lionrock were conducted by Nayak and Takemi (2019a, 2019b). The same model

212   configurations used in Nayak and Takemi (2019a, 2019b) were integrated in this study but with

213   four nested domains. Takemi (2018) used a horizontal grid spacing of 167 m to simulate the

214   heavy rainfall event that occurred in the northern part of Kyushu Island in July 2017 and

215   indicated that the 167-m grid simulation quantitatively captured the rainfall amount. Takemi and

216   Ito (2020) examined the ability to represent strong winds due to typhoons in complex terrain

217   with a horizontal grid spacing of 200 m and indicated that the wind speeds simulated with a grid

218   spacing of 200 m were quantitatively estimated better than those simulated with a grid spacing of

219   1 km. In this way, both studies demonstrated that the grid spacing on the order of 100 m

220   adequately captured the spatial and temporal variability of rainfall and wind in complex terrain.

221   In this study, we took advantage of high-resolution simulations with a grid spacing on the order

222   of 100 m. The initial and boundary conditions for the WRF simulations were provided from the

223   Japanese Reanalysis (JRA55) dataset. For the calculation of precipitation, the 1-km Radar-

224   AMeDAS precipitation data were downscaled to 200 m resolution by using the nearest

225   neighbour interpolation technique with the help of CDO (Climate Data Operators) software

11

226   (CDO, 2019). The interpolation was based on the YAC (Yet Another Coupler) software package

227   (Hanke et al., 2016).

228   Topex (Miller et al., 1987) and slope angle were calculated using a digital elevation

229   model with a 10-m resolution (Geospatial Information Authority of Japan) by QGIS2.18.26

230   (QGIS Development Team, 2018) and GRASS7.4.3 (GRASS Development Team, 2018). Slope

231   angle under 5º corresponds to 9 % in slope steepness meaning gentle, the slope angle over 35º

232   corresponds to 70% in slope steepness meaning steep slope, between 5 º and 35 º corresponds to

233   between 9 % and 70% meaning moderate and strong slope. The distance-limited topex is the sum

234   of the elevation angles (above the horizon) or depression angles (below the horizon) estimated at

235   specified intervals on straight lines radiating outward from the target point in eight directions. A

236   positive topex value indicates sheltered topography (valley), a value of 0 indicates a flat plain,

237   and a negative value indicates exposed topography (ridge). We used line lengths of 1, 2, and 3

238   km, with measurement intervals of 100 m based on Lanquaye-Opoku and Mitchell (2005) and

239   Mitchell et al. (2001). Forest stand features immediately before the typhoons were derived from

240   the forest inventory data investigated in 2013 (Hokkaido Regional Forest Office).

241

242   *2.5 Modelling and validation*

243   Forest disturbance by typhoons was modelled as a function of the 17 explanatory variables

244   described above and 2 spatial variables (i.e., latitude and longitude) using GBDTs. Spatial

245   variables were included in the model to capture spatial autocorrelations that were not explained

246   by other variables.

247   The machine learning method is a powerful tool for variable selection, and it is

248   particularly suited to handling prediction problems that include nonlinear relationships between

12

249   predictor and response variables and complex interactions between variables (Sandri and

250   Zuccolotto, 2006; Strobl et al., 2007). Gradient boosting is an ensemble learning method that

251   sequentially combines multiple weak learners (in our case, decision trees) that are developed

252   with gradual emphasis on observations poorly predicted by the current ensemble model. This

253   technique permits the development of a model with a high predictive performance without

254   overfitting, in which high dimensional interactions among explanatory variables and nonlinear

255   responses are fully accounted for. Interpretation of GBDTs is not as simple as conventional

256   methods such as generalized linear models, but several techniques, including individual

257   conditional expectation (ICE) plots and Friedman's H statistics, have recently been developed to

258   compensate for these shortcomings. According to these advantages, in forestry, gradient boosting

259   has been frequently used for modelling stand volume (Dube et al., 2015), canopy cover (Freeman

260   et al., 2015), and species distribution (Elith et al. 2008).

261   The following candidate values were tested for the GBDT models: 3, 5, and 10 for the

262   maximum depth of variable interactions for each learner; 5, 10, and 20 for the minimum number

263   of observations in the terminal nodes for each learner; 0.5 and 0.8 for the proportion of training

264   data used to build each learner; and 400, 600 and 800 for the total number of learners. The

265   shrinkage parameter was set to 0.01 during model assembly. The optimal parameters were

266   determined using spatially blocked 10-fold cross validation, and model predictive performance

267   was evaluated using Matthew's correlation coefficient (MCC) for the optimum threshold.

268   Accuracy and AUC were also calculated, although the optimal parameter was determined using

269   MCC.

270   The relative importance of explanatory variables was evaluated as a decrease in MCC

271   after permutation of a variable (Breiman, 2001). The average and context-dependent effects of

13

272   each explanatory variable on the probability of forest disturbance were visually inspected by a

273   partial dependence plot (Friedman, 2001) and ICE plot (Goldstein et al., 2015), respectively. The

274   ICE plot visualizes the effect of a given explanatory variable for each observation by connecting

275   the outcome of a model while shifting the values of the focal explanatory variable throughout the

276   range while keeping other explanatory variables as the original value. The partial dependence

277   plot indicates the average trend of each curve in the ICE plot. For the ICE plot, each line was

278   centred at zero at the left end of the x-axis to show the relative effects of explanatory variables

279   (c-ICE plot *sensu* (Goldstein et al., 2015)). Each line in the ICE plot was coloured based on the

280   value of the second explanatory variable to assist with the assessment of the interactive effects of

281   the two predictors. Friedman's H statistic (Friedman and Popescu, 2008) was used to detect

282   explanatory variables whose interaction with the vegetation variables was important and

283   therefore should be used for colour-coding of an ICE plot. Friedman's H is defined as a

284   proportion of the variance in partial dependence estimates explained by interactive effects for

285   arbitrary suites of explanatory variables. Three hundred sites were randomly sampled for the ICE

286   plot to prevent the plots from being too dense.

287

288   **3 Results**

289   Most of the model performance indices (MCC=0.70, AUC=0.92, Accuracy=0.89) were

290   reasonably high compared with those of previous studies (Hanewinkel et al., 2004: MCC=0.16-

291   0.20, accuracy=0.65-0.70, Morimoto et al., 2019: MCC=0.28, AUC=0.93, accuracy=0.88).

292   Fig. 2 shows the importance of the predictor variables from gradient boosting for

293   predicting forest disturbance by typhoons. The three most important variables excluding spatial

294   variables that were influential on the forest disturbance were dominant species, relative slope

14

295   direction, and total precipitation. The maximum wind speed itself had low importance on the

296   prediction because it was highly correlated with topex (3 km) (Spearman's rho = -0.42), which

297   was ranked as the 6th most important variable for predicting the forest disturbance. Topex (3 km)

298   has two effects on forest disturbance: one is the sidelong effect that appears through the

299   maximum wind speed (the wind speed is higher in ridges; therefore, forest disturbance risk rises

300   there), and the other is the sheer effect of topography represented by topex (3 km) (strong winds

301   blow through while keeping the wind speed at the ridge, and turbulence occurs at the leeward

302   side of the ridge; therefore, forest disturbance is more likely to occur on the side than in the

303   valleys and slopes that experienced the same wind speed). Topex (3 km), which can explain both

304   the effects of wind speed and topography, is more likely to be selected as an effective variable

305   than the maximum wind speed. Once topex (3 km) is selected, the maximum wind speed alone

306   does not have much influence on the forest disturbance.

307   When we discuss the effect of a factor, we should consider its interaction with other

308   factors. Friedman's H, which indicates the strength of an interactive effect with other variables,

309   was high for dominant species, relative slope direction, and total precipitation (Fig. 3a), which all

310   have relatively high variable importance (Fig. 2). Dominant species moderately interacted with

311   total precipitation (Fig. 3b), and the relative slope direction moderately interacted with dominant

312   species (Fig. 3c) because the proportion of the variance explained by the interactive effects was
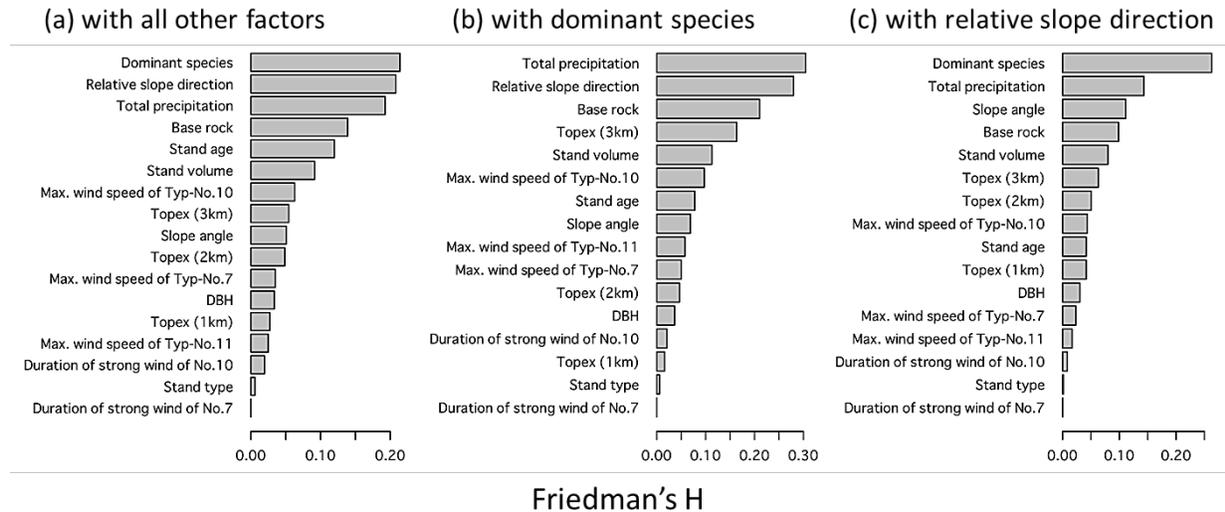
313   approximately 0.25 to 0.3.

15
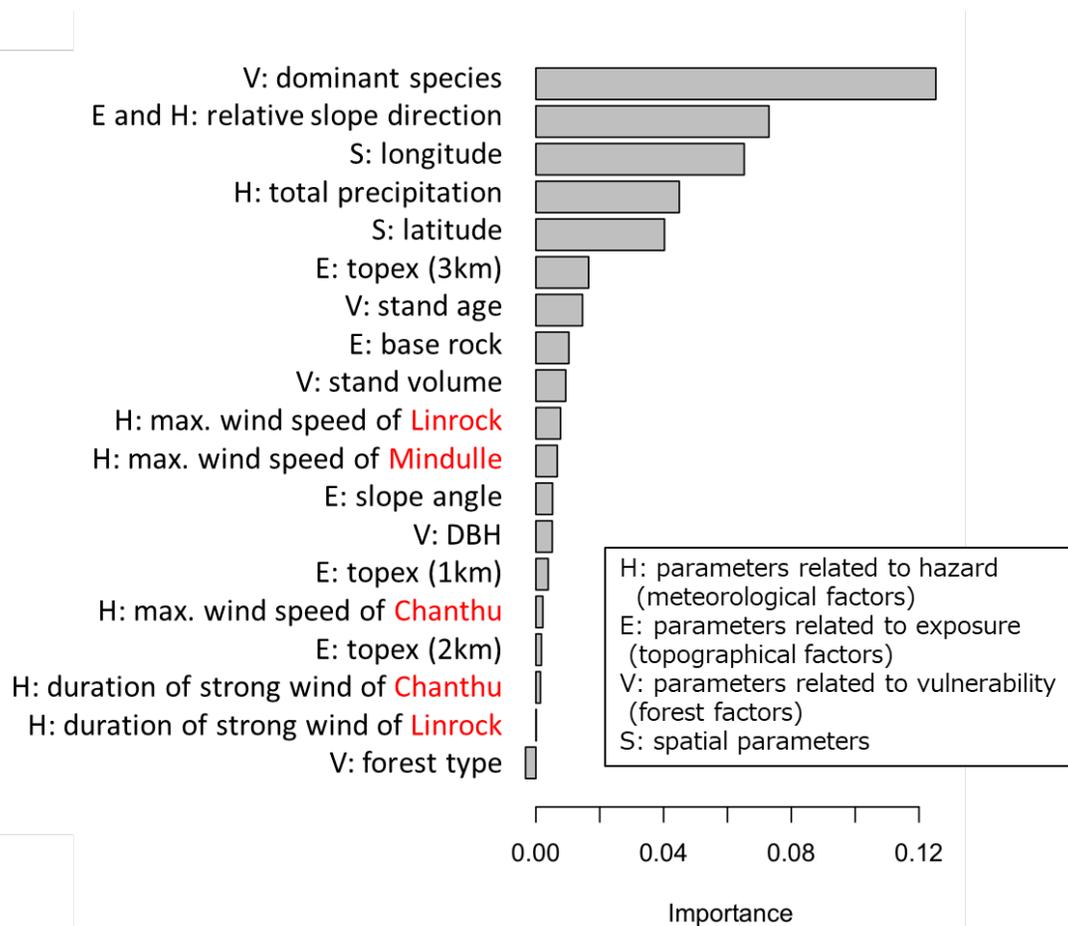
Fig. 2. Variable importance plots for predictor variables from gradient boosting for predicting the forest disturbance by typhoons.

16

(a) with all other factors   (b) with dominant species   (c) with relative slope direction

Friedman's H

Fig. 3. Friedman's H-statistics of each factor (a) with all other factors, (b) with dominant species, and (c) with relative slope direction for a model predicting the forest disturbance probability.

The partial plot showed the highest probability of disturbance in the *A. sachalinensis* stand among the main stands of five dominant species in the study area when other variables were fixed (Fig. 3a). A strong wind blowing from the front side of the slope showed a high probability of disturbance, regardless of the angle (Fig. 3b). The closer the wind direction was to the back of the slope, the lower the risk of disturbance. The probability of forest disturbance increased in stages when the total precipitation reached 60 mm and 100 mm (Fig. 4c). The probability of forest disturbance was higher in the ridge than in the flat and valley zones at the topography scale of 3 km (Fig. 4d).

17
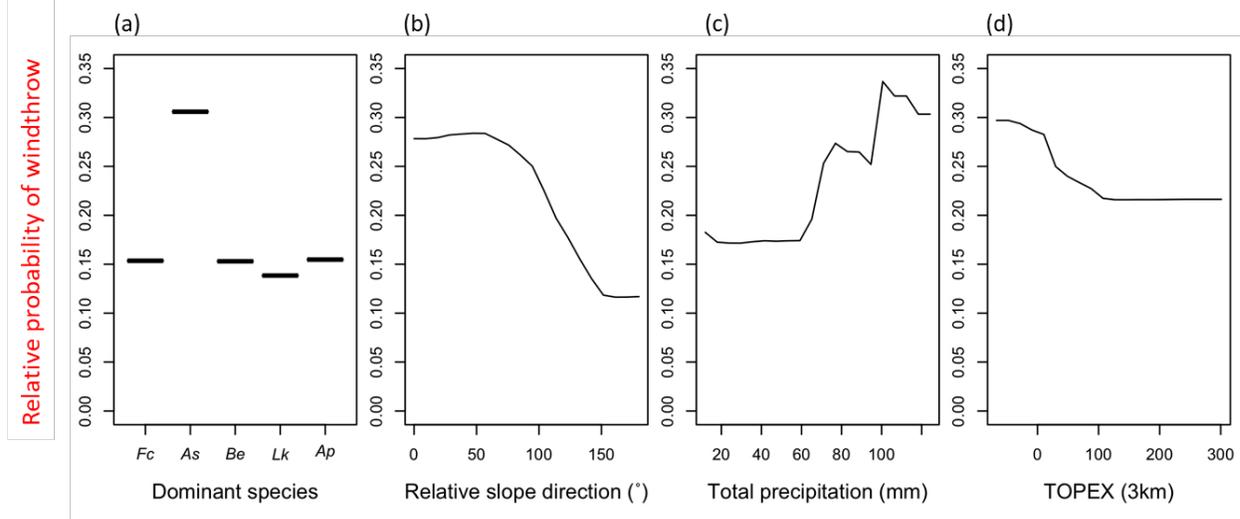
Fig. 4. Partial dependence plots for major predictor variables for GBDT predictions of forest disturbance occurrence; (a) dominant species (Fc (*Fagus crenata*), As (*Abies sachalinensis*), Be (*Betula ermanii*), Lk (*Larix kaempferi*), Ap (*Acer pictum*)), (b) relative slope direction (°), (c) total rainfall (mm), and (d) topex (3 km). Each plot is drawn in only the range or ranges of the subsample used for modelling.

The increasing pattern of the forest disturbance probability associated with the increasing total precipitation was different depending on the dominant species of the stands (Fig. 5). The disturbance probability of *A. sachalinensis* stands increased sharply when the total rainfall exceeded 60 mm. The stands of other dominant species showed a lower disturbance probability than *A. sachalinensis* stands in the total precipitation stage from 60 mm to 80 mm. Although sharp increases in disturbance probability were also observed for other species when total rainfall was > 100 mm, these responses are not very reliable or applicable due to the limited number of sites that experienced such high rainfall.

18

345
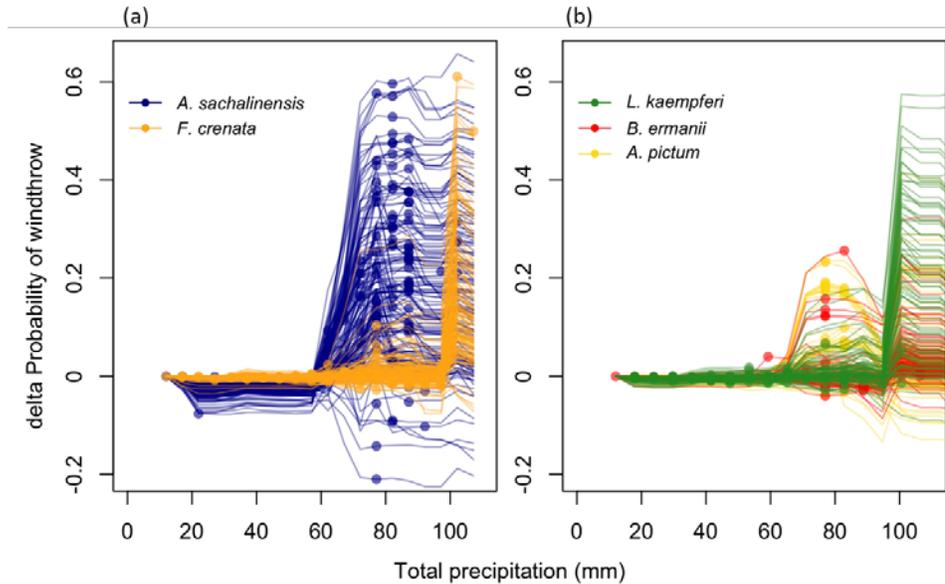
Fig. 5. Mutual effects between species and total precipitation on the probability of forest

disturbance. (a) *A. sachalinensis* and *F. crenata;* (b) *A. pictum, B. ermanii,* and *L. kaempferi.*

Expected responses for each grid were centred at zero at the low end of an explanatory variable.

Filled circles indicate observed values of an explanatory variable for each site. Three hundred

sites were randomly sampled for visualization to prevent the plots from being too dense.

351

4 Discussion

353

4.1 Feature of forest disturbance by typhoon accompanied by heavy precipitation

We confirmed two types of behaviours of the model: one represents the same process as that of

forest disturbance by strong wind, which has been widely studied, and another represents a

unique process mediated by storms and precipitation, which has not been investigated. The

former type of forest disturbance can occur in the early periods of typhoon landing and the latter

type of forest disturbance can occur in the late periods because the cumulative rainfall increases

as time passes.

19

361   Ridges exhibited a high risk of forest disturbance (Fig. 4d), as indicated in many previous

362   studies (Everham and Brokaw, 1996; Kramer et al., 2001), suggesting that strong winds

363   predominantly blew across valleys and caused stronger wind speeds at ridges than valleys (Ruel

364   et al., 1998) during typhoon landings. The effects of topography on the forest disturbance

365   probability actually included the effects of maximum wind speed, as a strong correlation was

366   indicated between topex (3k) and maximum wind speed. In addition, the decreasing pattern of

367   forest disturbance probability along with the increasing relative slope direction (Fig. 4b)

368   explained the contrasting damages across ridges due to the high variety of combinations in the

369   direction of the strong wind and the slope aspect in mountainous landscapes (Rentch, 2010). Our

370   analysis more specifically explained the old assertion that local unique topography increases the

371   probability of windthrow due to complex terrain (Ruel et al., 1998; Kramer et al., 2001).

372   Precipitation was shown to increase the risk of forest disturbance in forest stands, and its

373   effect was dependent on the dominant species of the stands. Total precipitation over 60 mm

374   during typhoon periods highly contributed to the forest disturbance (Fig. 2, Fig. 4c). Although

375   not all the total rainfall penetrated the soil and contributed to uprooting, it suggests that there was

376   some correlation with the amount of rainfall that substantially contributed to uprooting. This

377   result corresponds to a previous report that stated that tree stability was lower after rainfall (1 day

378   after 68 mm of precipitation along with a typhoon) than before (Koizumi, 1987), which was

379   confirmed by the tree-pulling test for five trees. In general, uniform structured forests such as

380   plantations are more vulnerable to storms than are multistoried natural forests (Quine and

381   Gardiner, 2007; Morimoto et al., 2019). However, the effect of the dominant species was more

382   important than that of the forest type (plantation or natural) in our model, suggesting that the tree

383   form representing the species features controls the process of forest disturbance in the case of

20

384   rain typhoons.

385   In general, thick and long taproots have the effect of anchor, avoiding from uprooting

386   (Karizumi, 2010). However, the anchor effect was not exerted under the rainy typhoon, given *A.*

387   *sachalinensis* whose taproot highly developed (Supplementary material S3) uprooted at lower

388   level of precipitation than other species. Interestingly, *A. sachalinensis* has a higher tendency in

389   uprooting by strong wind from the perspective of physical structure in root systems and canopy

390   traits (Supplementary material S3) showed high vulnerability to precipitation (Fig. 5); other

391   species that have a lower tendency in uprooting from the perspective of physical structure

392   showed mostly high resistance to precipitation. In particular, we noticed a lower density of

393   lateral and fine roots in *A. sachalinensis* than in other species. This result corresponded to the

394   previous suggestions that the horizontal distribution of root systems should serve as the major

395   resistance to windthrow (Krause et al., 2014), and few large trees can rely solely on tap roots and

396   need to develop thick lateral roots to prevent uprooting (Crook and Ennos, 1998).

397   The allometry of tree height with respect to the trunk diameter (height/DBH) has been

398   discussed as one of the most important factors determining windthrow damage (Cremer et al.,

399   1982; Ancelin et al., 2004). This parameter in the present study area ranged from 54 to 86 and 53

400   to 83 for *A. sachalinensis* and *L. kaempferi*, respectively. These ranges indicate the windthrow

401   risk from low to high according to Shibuya et al. (2011). Moreover, the ranges of allometry

402   values were similar for the two species, meaning that this factor cannot explain the difference in

403   vulnerability to precipitation, although this is one of the factors often related to treefalls by

404   typhoons.

405

406   ***4.2 Hypothesis of the forest disturbance process mediated by storm and precipitation***

21

407   The general process of treefall elucidated by tree-pulling experiments (Coutts, 1986; Karizumi,

408   2010; Kamimura et al., 2012) and the shapes of the root system related to resistance to

409   windthrow (Krause et al., 2014) provide us with the opportunity to form a hypothesis on how the

410   forest disturbance process is mediated by storms and precipitation inferred from the modelling

411   results. We focused on the process of uprooting because it was the dominant type of damage after

412   the events, and it has been reported that uprooting was identified under wet conditions more than

413   stem snapping when 16 studies of wind disturbance were compared (Peterson and Pickett, 1991).

414   Three types of interspaces will emerge in the soil around tree root systems when a tree is

415   attacked by strong wind (Supplementary Material S4a): the first is a small hollow hole between

416   roots and the adhering soil (Karizumi, 2010), the second is a complex network of cracks

417   developed on the windward edge of the root-soil plate, and the third is an irregular crack that

418   appears under the root-soil plate, apparently as a result of stretching the undersurface of the plate

419   and separation of the sinker roots (Coutts, 1986). Rainwater penetrates all of these gaps and

420   ultimately contributes to increasing the water content below the root-soil plate. The water content

421   below the root plate significantly affects root anchorage, i.e., high water content below the root

422   plate decreases root anchorage (Kamimura et al., 2012), which will then cause the tree to fall

423   over. The difference in vulnerability to rainfall may stem from the shape of the root system,

424   especially the volume of lateral roots, which serves as the major resistance to uprooting (Krause

425   et al., 2014). Dense lateral roots and fine roots will be able to widely disperse rainwater inside

426   the soil-root plate and postpone rainwater pooling under the plate. However, sparse lateral roots

427   and fine roots with thick taproots may gather most of the rainwater into cracks formed just below

428   the taproot, and the water content under the root plate may rise immediately (Supplementary

429   Material S4a). The root system of *A. sachalinensis* (Supplementary Material S4b), which had a

22

430   physical structure that was more likely to be uprooted by strong winds than other tree species,

431   also had root systems in which the soil water content under the root plate easily increased by

432   heavy rain (Supplementary Material S4b). Therefore, the difference among species in the risk of

433   forest disturbance appeared clearly.

434   This hypothesis should be verified by future tree-pulling experiments under artificial rain

435   and modelling the tree behaviour under storm and rain conditions.

436

437   *4.3 Effective solutions in forest management to decrease the risk in silviculture*

438   Forest disturbance risk modelling comprised of three main drivers (Oppenheimer et al., 2014)

439   helps us to examine what kind of factors related to exposure and vulnerability are to be managed

440   to effectively decrease the risk in silviculture in the situation of uncontrollable hazards in the

441   future. Regarding controlling exposure, avoiding silviculture on a ridge is recommended

442   considering that the risk estimated in this area was higher not only in our study but also in many

443   previous windthrow models (for example, Mitchell, 2013). In addition to controlling exposure,

444   vulnerability control is also important. In our model, dominant tree species were related to forest

445   disturbance through vulnerability to rainfall. Species having dense lateral roots would be suitable

446   for planting because they may have higher resistance to typhoons accompanied by heavy rain.

447   However, we must admit the limitation of our analyses. Our modelling only expresses the pattern

448   or process that a major trend shows because all variables are simulated or estimated. Then, we

449   cannot discuss the minor trend of forest disturbance. Additionally, the high importance of latitude

450   and longitude in our model (Fig. 2) means that there are still missing spatial variables that are

451   strongly related to forest disturbance by typhoons, although we tried to include all the possible

452   factors we could evaluate. We might determine a more specific process of forest disturbance by

23

453   typhoons accompanied by heavy precipitation after including new principal parameters.

454

455

456

469

470   **Declarations of interest**

471   None

472

473   **Data availability**

474   The datasets presented in this article are not readily available because they contain forest

475   inventory data restricted by the Hokkaido Regional Forest Office of Forestry Agency and

476   Hokkaido Government's Bureau of Forestry. Requests to access the datasets should be directed

477   to Junko Morimoto.

478

References

479 **References**

480 Ancelin, P., Courbaud, B., Fourcaud, T., 2004. Development of an individual tree-based

481   mechanical model to predict wind damage within forest stands. For. Ecol. Manag. 203,

482   101–121. https://doi.org/10.1016/j.foreco.2004.07.067.

483 Bureau of Forestry, Department of Fisheries and Forestry, Hokkaido Government, 2018.

484   Growing forests to reduce the risk of damage of windthrow. 8pp. in Japanese.

485   http://www.pref.hokkaido.lg.jp/sr/srs/riskdown.pdf.

486 Busgen, M., Munch, E., 1929. The structure and life of forest trees, Chapman and Hall Limited,

487   London, UK.

488 Breiman, L., 2001. Random forests. Mach. Learn. 45, 5–32.

489   https://doi.org/10.1023/A:1010933404324.

490 Congedo, L., 2016. Semi-Automatic Classification Plugin Documentation.

491   https://doi.org/10.13140/RG.2.2.29474.02242/1.

492 Coppin, P.R., Bauer, M.E., 1996. Digital Change Detection in Forest Ecosystems with Remote

493   Sensing Imagery. Remote Sens. Rev. 13, 207–234.

494   https://doi.org/10.1080/02757259609532305.

495 Guangxing Wang, Q.W., 2013. Remote Sensing of Natural Resources, 1st ed. Taylor & Francis.

496 Coutts, M.P., 1986. Components of tree stability in sitka spruce on peaty gley soil. For. Int. J.

497   For. Res. 59, 173–197. https://doi.org/10.1093/forestry/59.2.173.

498 Cremer, K.W., Borough, C.J., McKinnell, F.H., Carter, P.R., 1982. Effects of stocking and

499   thinning on wind damage in plantations. N. Z. J. For. Sci. 12, 244–268.

500 Crook, M.J., Ennos, A.R., 1998. The increase in anchorage with tree size of the tropical tap

501   rooted tree mallotus wrayi , king (*Euphorbiaceae*). Ann. Bot. 82, 291–296.

502   https://doi.org/10.1006/anbo.1998.0678.

503   Dou, J., Yunus, A. P., Xu, Y., Zhu, Z., Chen, C., Sahana, M., Khosravi, K., Yang, Y., Pham, B. T.,

504   2019. Torrential rainfall-triggered shallow landslide characteristics and susceptibility

505   assessment using ensemble data-driven models in the Dongjiang Reservoir Watershed,

506   China, Natural Hazards. 97:579–609. https://doi.org/10.1007/s11069-019-03659-4.

507   Dube, T., Mutanga, O., Abdel-Rahman, E.M., Ismail, R., Slotow, R., 2015. Predicting Eucalyptus

508   spp. stand volume in Zululand, South Africa: an analysis using a stochastic gradient

509   boosting regression ensemble with multi-source data sets. International Journal of

510   Remote Sensing. 36:14, 3751-3772, DOI: 10.1080/01431161.2015.1070316.

511   Elith, J., Leathwick, J.R., Hastie, T., 2008. A working guide to boosted regression trees. J Anim

512   Ecol. 77, 802–813. https://doi.org/10.1111/j.1365-2656.2008.01390.x.

513   Everham, E.M., Brokaw, N.V.L., 1996. Forest damage and recovery from catastrophic wind. Bot.

514   Rev. 62, 113–185. https://doi.org/10.1007/BF02857920.

515   Freeman, E.A., Moisen, G.G., Coulston, J.W., Wilson, B.T., 2015. Random forests and stochastic

516   gradient boosting for predicting tree canopy cover: comparing tuning processes and

517   model performance. dx.doi.org/10.1139/cjfr-2014-0562.

518   Friedman, J.H., 2001. Greedy function approximation: a gradient boosting machine. Ann. Stat.

519   29, 1189–1232. https://doi.org/10.1214/aos/1013203451.

520   Friedman, J.H., Popescu, B.E., 2008. Predictive learning via rule ensembles. Ann. Appl. Stat. 2,

521   916–954. https://doi.org/10.1214/07-AOAS148.

522   Goldstein, A., Kapelner, A., Bleich, J., Pitkin, E., 2015. Peeking inside the black box: visualizing

523   statistical learning with plots of individual conditional expectation. J. Comput. Graph.

524   Stat. 24, 44–65. https://doi.org/10.1080/10618600.2014.907095.

525   GRASS Development Team, 2018. Geographic Resources Analysis Support System (GRASS)

526   software. Open Source Geospatial Foundation. http://grass.osgeo.org/(accessed 29 May

527   2020).

528   Hanewinkel, M., Kuhn, T., Bugmann, H., Lanz, A. Brang, P., 2014. Vulnerability of uneven-aged

529   forests to storm damage. Forestry. 87:4, 525–534. doi:10.1093/forestry/cpu008.

530   Hanke, M., Redler, R., Holfeld, T., Yastremsky, M., 2016. YAC 1.2. 0: new aspects for coupling

531   software in earth system modelling. Geosci. Model Dev. 9, 2755–2769.

532   https://doi.org/10.5194/gmd-9-2755-2016.

533   Jalkanen, A., Mattila, U., 2000. Logistic regression models for wind and snow damage in

534   northern Finland based on the national forest inventory data. For. Ecol. Manag. 135, 315–

535   330. https://doi.org/10.1016/S0378-1127(00)00289-9.

536   Japan Meteorological Agency, 2017. Disaster Meteorological Report - Heavy Rain and Storms

537   from 2016 August 16 to August 31 due to Typhoon No. 7, No. 9, No. 10, No. 11 and

538   Front Line in 2016. Natural Disaster Report, Japan.

539   Kamimura, K., Kitagawa, K., Saito, S., Mizunaga, H., 2012. Root anchorage of hinoki

540   (*Chamaecyparis obtuse (Sieb. Et Zucc.) Endl.*) under the combined loading of wind and

541   rapidly supplied water on soil: analyses based on tree-pulling experiments. Eur. J. For.

542   Res. 131, 219–227. https://doi.org/10.1007/s10342-011-0508-2.

543   Karizumi, N., 2010. The Latest Illustrations of Tree Roots. Seibundo Shinkosha Publishing Co.,

544   Ltd., Hongo Bunkyo-Ku, Tokyo.

545   Koizumi, A., 1987. Studies on the estimation of the mechanical properties of standing trees by

546   non-destructive bending test. Res. Bull. Coll. Exp. For. Hokkaido Univ. 44, 1329–1415.

547   Koizumi, A. Motoyama, J., Sawata, K., Sasaki, Y., Hirai, T., 2010. Evaluation of drag

548   coefficients of poplar-tree crowns by a field test method. Journal of Wood Science. 56:3,

549   189-193. 10.1007/s10086-009-1091-8.

550   Kruse, F.A., Lefkoff, A.B., Boardman, J.W., Heidebrecht, K.B., Shapiro, A.T., Barloon, P.J.,

551   Goetz, A.F.H., 1993. The spectral image processing system (SIPS)-interactive

552   visualization and analysis of imaging spectrometer data. Remote Sens. Environ. 44, 145-

553   163. https://doi.org/10.1016/0034-4257(93)90013-N.

554   Kramer, M.G., Hansen, A.J., Taper, M.L., Kissinger, E.J., 2001. Abiotic controls on long-term

555   windthrow disturbance and temperate rain forest dynamics in southeast Alaska. Ecology

556   82, 2749–2768. https://doi.org/10.1890/0012-9658(2001)082[2749:ACOLTW]2.0.CO;2.

557   Krause, C., Lemay, A., Tremblay, S., Ruel, J.C., Plourde, P.Y., 2014. How does the root system

558   inhibit windthrow in thinned black spruce sites in the boreal forest? Trees 28, 1723–1735.

559   https://doi.org/10.1007/s00468-014-1080-4.

560   Kruse, F.A., Lefkoff, A.B., Boardman, J.W., Heidebrecht, K.B., Shapiro, A.T., Barloon, P.J.,

561   Goetz, A.F.H., 1993. The spectral image processing system (SIPS)—interactive

562   visualization and analysis of imaging spectrometer data. Remote Sens. Environ. 44, 145–

563   163. https://doi.org/10.1016/0034-4257(93)90013-N.

564   Lanquaye-Opoku, N., Mitchell, S.J., 2005. Portability of stand-level empirical windthrow risk

565   models. For. Ecol. Manag. 216, 134–148. https://doi.org/10.1016/j.foreco.2005.05.032.

566   Miller, K.F., Quine, C.P., Hunt, J., 1987. The assessment of wind exposure for forestry in Upland

567   Britain. For. Int. J. For. Res. 60, 179–192. https://doi.org/10.1093/forestry/60.2.179.

568   Mitchell, S.J., 2013. Wind as a natural disturbance agent in forests: a synthesis. For. Int. J. For.

569   Res. 86, 147–157. https://doi.org/10.1093/forestry/cps058.

570   Mitchell, S.J., Hailemariam, T., Kulis, Y., 2001. Empirical modeling of cutblock edge windthrow

571   risk on Vancouver Island, Canada, using stand level information. For. Ecol. Manag. 154,

572   117–130. https://doi.org/10.1016/S0378-1127(00)00620-4.

573   Mitchell, S.J., Ruel, J.C., 2015. Modeling windthrow at stand and landscape scales, in: Perera,

574   A.H., Sturtevant, B.R., Buse, L.J. (Eds.), Simulation Modeling of Forest Landscape

575   Disturbances. Springer International Publishing, Cham, pp. 17–43.

576   Morimoto, J., Nakagawa, K., Takano, K.T., Aiba, M., Oguro, M., Furukawa, Y., Mishima, Y.,

577   Ogawa, K., Ito, R., Takemi, T., Nakamura, F., Peterson, C.J., 2019. Comparison of

578   vulnerability to catastrophic wind between *Abies* plantation forests and natural mixed

579   forests in northern Japan. For. Int. J. For. Res. 92, 436–443.

580   https://doi.org/10.1093/forestry/cpy045.

581   Murakami, H., Wang, Y., Yoshimura, H., Mizuta, R., Sugi, M., Shindo, E., Adachi, Y., Yukimoto,

582   S., Hosaka, M., Kusunoki, S., 2012. Future changes in tropical cyclone activity projected

583   by the new high-resolution MRI-AGCM. J. Clim. 25, 3237–3260.

584   https://doi.org/10.1175/JCLI-D-11-00415.1.

585   Nakashizuka, T., 1989. Role of uprooting in composition and dynamics of an old-growth forest

586   in Japan. Ecology 70, 1273–1278. https://doi.org/10.2307/1938186.

587   Nayak, S., Takemi, T., 2019a. Dynamical downscaling of Typhoon Lionrock (2016) for assessing

588   the resulting hazards under global warming. J. Meteorol. Soc. Jpn. 97, 69–88.

589   https://doi.org/10.2151/jmsj.2019-003.

590   Nayak, S., Takemi, T., 2019b. Quantitative estimations of hazards resulting from Typhoon

591   Chanthu (2016) for assessing the impact in current and future climate. Hydrol. Res. Lett.

592   13, 20–27. https://doi.org/10.3178/hrl.13.20.

593   Oppenheimer, M., Campos, M., Warren, R., Birkmann, J., Luber, G., O'Neill, B., Takahashi, K.,

594   Berkhout, F., Dube, P., Foden, W., Greiving, S., Hsiang, S., Johnston, M., Keller, K.,

595   Kleypas, J., Kopp, R., Licker, R., Peres, C., Price, J., Robock, A., Schlenker, W., Stepp,

596   J.R., Tol, R., van Vuuren, D., 2014. Emergent risks and key vulnerabilities, in: Field,

597   C.B., Barros, V.R., Dokken, D.J., Mach, K.J., Mastrandrea, M.D., Bilir, T.E., Chatterjee,

598   M., Ebi, K.L., Estrada, Y.O., Genova, R.C., Girma, B., Kissel, E.S., Levy, A.N.,

599   MacCracken, S., Mastrandrea, P.R., White, L.L. (Eds.), Climate Change 2014 Impacts,

600   Adaptation, and Vulnerability Part A: Global and Sectoral Aspects Working Group II

601   Contribution to the Fifth Assessment Report of the Intergovernmental Panel on Climate

602   Change. Cambridge University Press, Cambridge, United Kingdom and New York, NY,

603   USA, pp. 1039–1100.

604   Peterson, C.J., Pickett, S.T.A., 1991. Treefall and resprouting following catastrophic windthrow

605   in an old-growth hemlock-hardwoods forest. For. Ecol. Manag. 42, 205–217.

606   https://doi.org/10.1016/0378-1127(91)90025-Q.

607   Planet Lab Inc., 2020. PLANET IMAGERY AND ARCHIVE [WWW Document].

608   https://www.planet.com/products/planet-imagery/ (accessed 7.3.20).

609   QGIS Development Team, 2018. QGIS geographic information system. Open Source Geospatial

610   Foundation Project. http://qgis.osgeo.org (accessed 29 May 2020).

611   QGIS.org, 2020. QGIS Geographic Information System [WWW Document]. Open Source

612   Geospatial Found. Proj. https://www.qgis.org (accessed 13 July 2020).

613   Quine, C.P., Gardiner, B.A., 2007. Understanding how the interaction of wind and trees results in

614   windthrow, stem breakage, and canopy gap formation, in: Johnson, E.A., Miyanishi, K.

615   (Eds.), Plant Disturbance Ecology. Academic Press, Burlington, pp. 103–155.

616   Sandri, M., Zuccolotto, P., 2006. Variable selection using random forests. In Data Analysis,

617   Classification and the Forward Search: Proceedings of the Meeting of the Classification

618   and Data Analysis Group (CLADAG) of the Italian Statistical Society, University of

619   Parma, June 6–8, 2005. Zani S., Cerioli A., Riani M. and Vichi M. (eds). Springer Berlin

620   587 Heidelberg, pp. 263–270.

621 Strobl, C., Boulesteix, A.-L., Zeileis, A., Hothorn, T. 2007. Bias in random forest variable

622   importance measures: illustrations, sources and a solution. BMC Bioinformatics. 8:1, 25.

623   doi:10.1186/1471-2105-8-25.

624 Rentch, J., 2010. Relationship between treefall direction, slope-aspect, and wind in eight old-

625   growth oak stands in the central hardwood forest, USA. J. Torrey Bot. Soc. 137, 391–400.

626   https://doi.org/10.2307/25790860.

627 Ruel, J.C., Pin, D., Cooper, K., 1998. Effect of topography on wind behaviour in a complex

628   terrain. For. Int. J. For. Res. 71, 261–265. https://doi.org/10.1093/forestry/71.3.261.

629 Schulzweida, U., 2019. CDO User Guide (Version 1.9.8).

630   https://doi.org/10.5281/zenodo.3539275.

631 Shibuya, M., Urata, T., Torita, H., Iijima, H., 2011. Windthrow damage and tree shape in

632   coniferous plantations in central Hokkaido, northern Japan. Jpn. J. For. Environ. 53, 53–

633   59. https://doi.org/10.18922/jjfe.53.2_53.

634 Skamarock, W.C., Klemp, J.B., Jimy, D., David, O.G., Dale, B., Michael, G.D., Xiang-Yu, H.,

635   Wei, W., Jordan, G.P., 2008. Description of the Advanced Research WRF Version 3 (No.

636   NCAR/TN-475+STR). University Corporation for Atmospheric Research.

637 Stathers, R.J., Rollerson, T.P., Mitchell, S.J., 1994. Windthrow Handbook for British Columbia

638   Forests. Working Paper No. 9401. British Columbia Ministry of Forests, Victoria.

639 Takemi, T., 2019. Impacts of global warming on extreme rainfall of a slow-moving typhoon: a

640   case study for Typhoon Talas (2011). SOLA 15, 125–131.

641   https://doi.org/10.2151/sola.2019-023.

642 Takemi, T., Ito, R., 2020. Benefits of high-resolution downscaling experiments for assessing

643   strong wind hazard at local scales in complex terrain: a case study of Typhoon Songda

644   (2004). Prog. Earth Planet. Sci. 7, 1–16. https://doi.org/10.1186/s40645-019-0317-7.

645 Yamamoto, S.I., 1989. Gap dynamics in climaxFagus crenata forests. Bot. Mag. Shokubutsu-

646   Gaku-Zasshi 102, 93–114. https://doi.org/10.1007/BF02488116.

647